Giant Helical Dichroism of Single Chiral Nanostructures with Photonic Orbital Angular Momentum

Jincheng Ni,[§] Shunli Liu,[§] Guangwei Hu, Yanlei Hu, Zhaoxin Lao, Jiawen Li,* Qing Zhang, Dong Wu,* Shaohua Dong, Jiaru Chu, and Cheng-Wei Qiu*

ACCESS | 📊 Metrics & More | 📖 Article Recommendations | 🆂🅸 Supporting Information

ABSTRACT: Optical activity, demonstrating the chiral light-matter interaction, has attracted tremendous attention in both fundamental theoretical research and advanced applications of high-efficiency enantioselective sensing and next-generation chiroptical spectroscopic techniques. However, conventional chiroptical responses are normally limited in large assemblies of chiral materials by circularly polarized light, exhibiting extremely weak chiroptical signals in a single chiral nanostructure. Here, we demonstrate that an alternative chiral freedom of light—orbital angular momentum—can be utilized for generating strong helical dichroism in single chiral nanostructures. The helical dichroism by monochromatic vortex beams can unambiguously distinguish the intrinsic chirality of nanostructures, in an excellent agreement with theoretical predictions. The single planar-chiral nanostructure can exhibit giant helical dichroism of ~20% at the visible wavelength. The vortex-dependent helical dichroism, expanding to single nanostructures and two-dimensional space, has implications for high-efficiency chiroptical detection of planar-chiral nanostructures in chiral optics and nanophotonic systems.

KEYWORDS: orbital angular momentum, planar chirality, helical dichroism, optical activity, chiral nanostructures
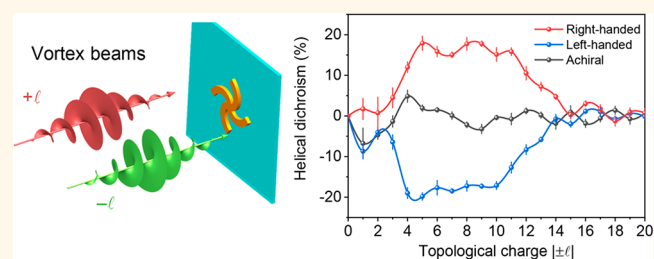
INTRODUCTION

Chirality, showing the geometric property of an object, which does not coincide with its mirror image, is quite ubiquitous in the physical world and has significant implications.[1] In nature, chiral molecules are essential to the functioning and continuation of biological processes, such as organic sugars, proteins, and nucleic acids.[2] Nowadays, various artificially chiral objects, created by advanced and sophisticated micro/nanofabrication techniques, have demonstrated excellent optical and mechanical properties by mimicking natural structures.[3−6] Distinguished from the geometric features, light waves naturally possesses intrinsic chiral characteristic by carrying angular momenta.[7,8] For example, circularly polarized light, carrying spin angular momentum (SAM), has two forms of handedness and exists helical electrical vectors along its propagating axis. Analogous to the SAM, an optical vortex with orbital angular momentum (OAM) also possesses handedness but unlimited OAM eigenvalues with helical phase wavefronts ($E \sim e^{il\varphi}$, where E is the complex electric field distribution, determined by the integer topological charge l, and the azimuthal angle of φ).[9−14]

Optical activity is a well-known phenomenon of the manifestation of chirality by light−matter interactions, which has been intensely studied in the past and still attracts tremendous attention in the field of modern optics.[7,15−18] Specifically, the chiroptical response has been predominately investigated by left- and right-handed circularly polarized light, which lays the foundations of various chiroptical technologies including polarization rotation and photoabsorption circular dichroism (CD).[19−21] Recently, the photonic OAM has also been proposed to involve in CD measurements,[22,23] generating chiroptical signals even in achiral nanostructures with spin−orbit interaction of light. However, the chiral light-matter interaction generated by only photonic OAM remains elusive, which is at the heart of the field of vortex-dependent chiroptical response.
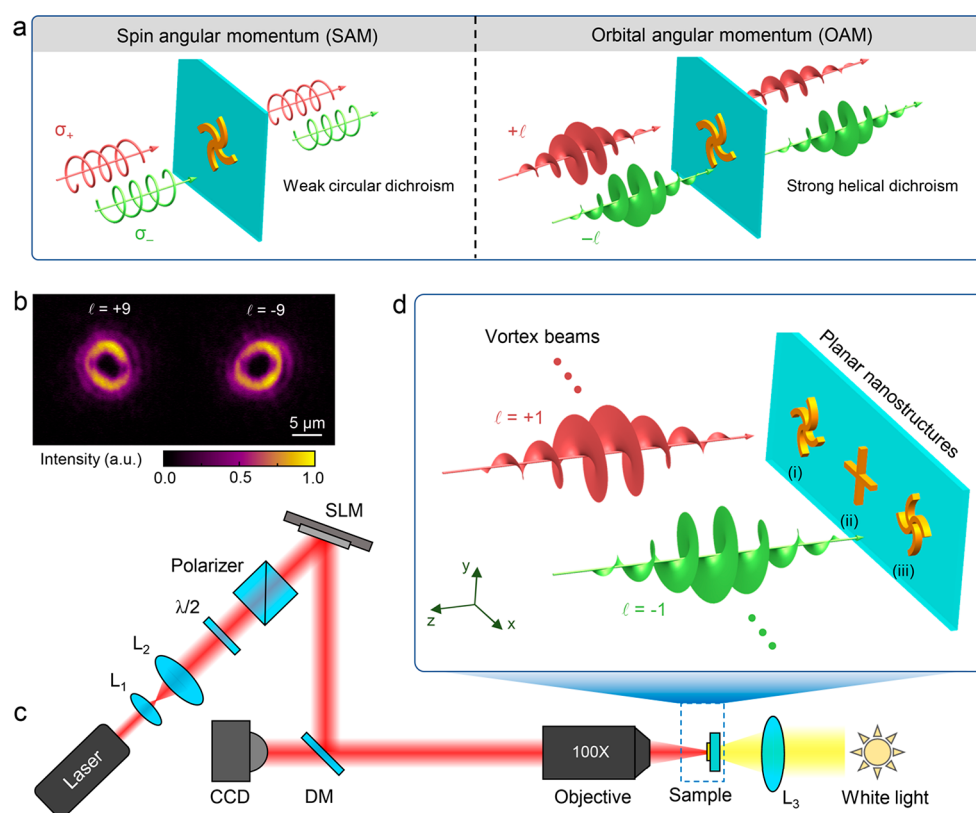
Figure 1. Concept of distinguishing single chiral nanostructures by vortex-assisted helical dichroism. (a) Schematic of chiroptical response on a single chiral nanostructure by photonic spin or orbital angular momentum. A single chiral nanostructure has a weak chiroptical signal of CD, whereas its HD signal is strong with the dimensional matching of helical phase and the structure. (b) Optical images of generated vortex beams with topological charges $l = +9$ and -9. (c) Optical setup utilized for measuring HD on single nanostructures. An expanded Gaussian light beam is modulated by a phase-only spatial light modulator (SLM) for generating vortex beams. Then the vortex beam with controllable topological charge is focused on the single planar nanostructures. The reflected light of nanostructures is collected by the same microscope objective. The CCD and the DM shown in the figure refer to a charge-coupled device camera and a dichroic mirror, respectively. (d) Schematic of the single right-handed (i), cross-shaped (ii), and left-handed nanostructures (iii) illuminated by tunable vortex beams at normal incidence.

Because of the weak chiroptical signals in natural biomolecules, many chiral metamaterials with unusual optical properties have been explored to yield conspicuous spin-related optical activity for miniaturized polarizers,[3,24,25] spin-controlled optical devices,[16,26] and nonlinear optics.[27−29] Typically, the chiroptical response originates from the intrinsic chirality in three-dimensional structures. However, recent experiments have also shown that planar metamaterials can obtain chiroptical properties by their lack of in-plane mirror symmetry (the so-called planar-chiral structures)[30−34] or illuminated at oblique incidence.[35,36] Although the pronounced CD signal in planar metamaterials has been realized with large amounts of chiral cells,[32,37] the chiroptical response is still extremely weak for a single planar-chiral nanostructure. To satisfy the ever-increasing demand for ultrasensitive chiral detection in next-generation chiroptical spectroscopy, a high-efficiency chiroptical approach of chiral matters in small quantities is clearly needed.

Here, we theoretically and experimentally demonstrate the giant helical dichroism (HD) in a single chiral nanostructure by optical vortices with photonic OAM. The vortex-dependent HD is experimentally validated on planar-chiral Archimedean nanospirals, consistent with numerical simulation results. The induced HD spectroscopy is mirror-symmetric for left- and right-handed nanospirals and has a maximum HD value of

$\sim$20% in single planar-chiral nanostructures. The chiroptical studies of single nanostructures via optical vortices can potentially facilitate the advanced chiroptical spectroscopy and programmable designs of planar-chiral nanostructures.

RESULTS AND DISCUSSION

Concept and Origin of Vortex-Dependent HD Measurement. The chiroptical properties of nanostructures by circularly polarized light predominantly depend on two parameters: the dielectric permittivity and the size parameters.[38,39] The incident circularly polarized light can be defined by the unitary vector $\sigma_{\pm} = (\mathbf{x} \pm i\mathbf{y})/\sqrt{2}$, where the sign refers to the photon helicity that is related to its polarized states. Chiral nanostructures can exhibit a strong Mie resonance with a comparable or smaller size to the operating wavelength.[4,40] However, a single chiral nanostructure normally demonstrates a weak CD signal due to the large structure size compared to the small operating wavelength (Figure 1a and more discussion in section S1). Distinguished from photonic SAM, the chiral properties of vortex beams are concealed in the winding phase distributions, which can match the dimensions of single structures for yielding giant HD signals.

The experimental setup is implemented for the chiroptical detection of planar-chiral nanostructures by vortex beams, as illustrated in Figure 1c. The vortex beams with controllable

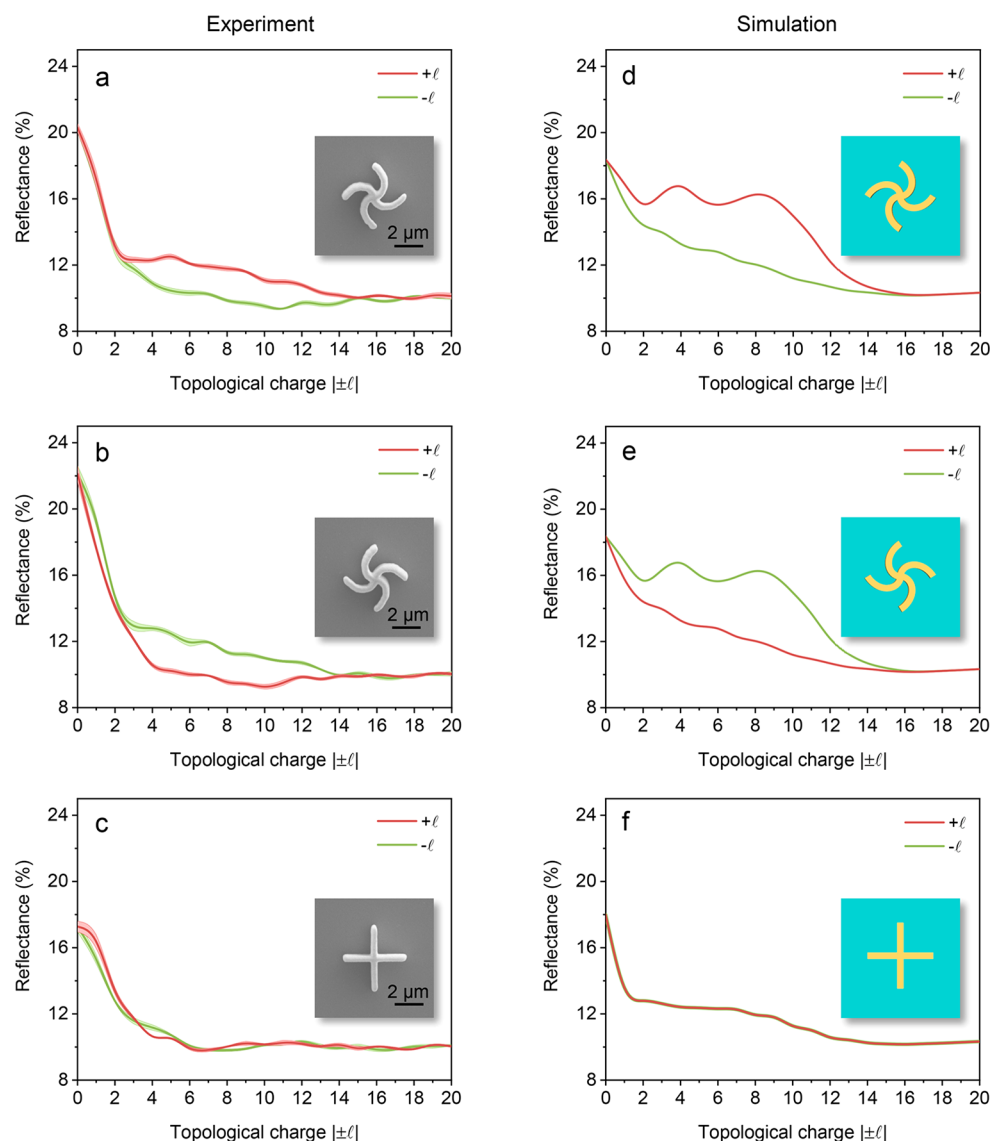Experiment   Simulation

Figure 2. Vortex-dependent reflectance difference on single nanostructures. Measured reflectance on right-handed (a), left-handed (b), and achiral cross-shaped (c) nanostructures by vortex beams with topological charge $|\pm l|$ from 0 to 20. Solid lines show the mean value and the shading indicates the standard deviation of multiple measurements. Insets are the corresponding scanning electron microscopy (SEM) images. (d−f) Simulated reflectance on single planar nanostructures corresponding to (a−c), respectively. All the planar nanostructures have identical thickness of 2 μm and line width of 420 nm.

topological charge l are generated by a phase-only spatial light modulator (SLM) with tunable fork holograms. Then the vortex beams propagating along the $-z$ direction are slightly focused on the sample with a microscopy objective (see Experimental Section). In this scenario, the linearly polarized vortex beams with helical phase wavefronts are illuminated on the single nanostructures at normal incidence, avoiding any disturbance from photonic SAM or extrinsic helicity from light beams.[23,35] The donut-shape intensity profiles of high-quality vortex beams can be caught by the charge-coupled device (CCD) camera, as shown in Figure 1b. The intrinsically chiroptical properties of planar nanostructures are demonstrated by the distinct reflectance for vortex beams with opposite topological charges (Figure 1d). The planar-chiral nanostructures are modeled by Archimedean spirals as a function of $r = 2/\pi \times r_{max} \times \mod(\theta, \pi/2)$, where r and θ are the polar coordinate system (see Figure S1). It is worth noting that the planar-chiral nanospirals are 4-fold rotational

symmetry (C_4) with respect to the z axis and are reciprocal for opposite-handed nanospirals.[31] An achiral cross-shaped nanostructure is also modeled with in-plane mirror-symmetry. We consider an incoming vortex beam propagating in $-z$ direction as

$$\boldsymbol{E}_I(\boldsymbol{r}, t) = \begin{pmatrix} I_{+l} \\ I_{-l} \end{pmatrix} e^{il\varphi} e^{i(-\boldsymbol{k}_0 z - \omega t)} \tag{1}$$

where $\boldsymbol{k}_0$ is the wavevector, ω is the frequency, and $I_{\pm l}$ describes the amplitude distributions of vortex beams with topological charges $\pm l$. Distinguishing from circularly polarization with only two states, the light can be projected on infinite-dimensional OAM eigenstates characterized by Hilbert factor $e^{il\varphi}$, which demonstrates as a digital spiral spectrum.[41] Theoretically, the vortex-assisted HD spectra obeys the mirror-symmetric properties for left- and right-handed nanostructures (see Section S2). The insights of vortex-dependent chiral light-
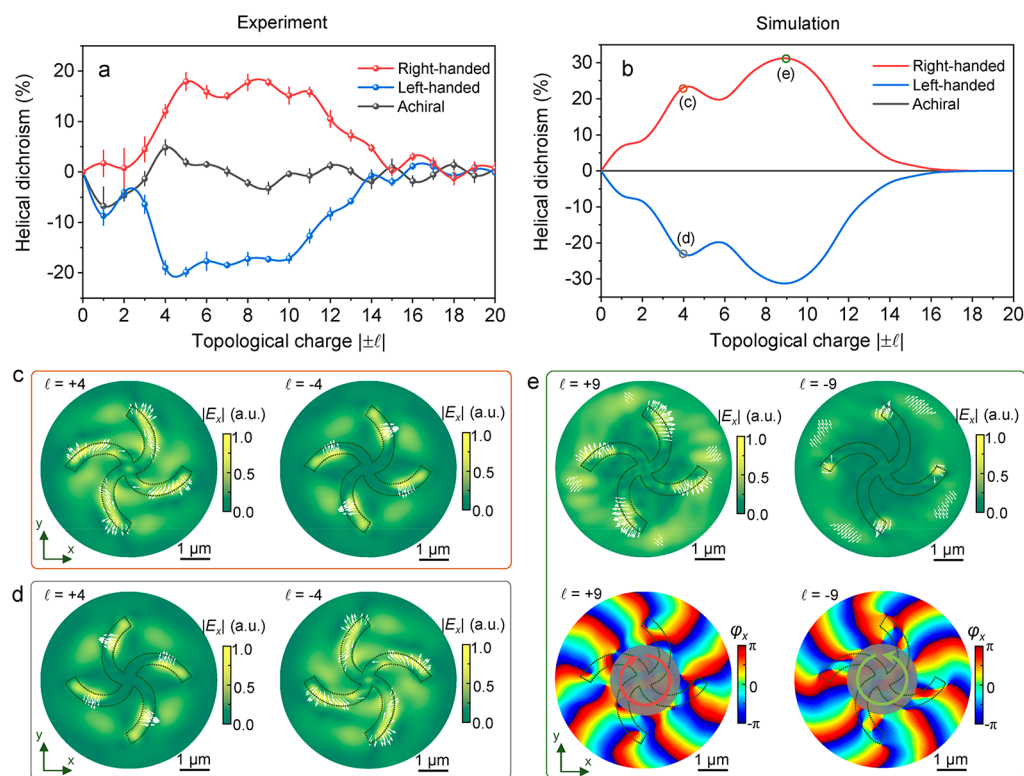
Figure 3. Helical dichroism of planar nanostructures by vortex beams. Measured (a) and simulated (b) HD spectra on the single planar nanostructures. Electric field distributions of right- (c) and left-handed (d) nanospirals under vortex beams with topological charges $l = \pm 4$. White arrows indicate the Poynting vectors. The $x-y$ planes of simulated electric fields are located at the middle of nanostructures. (e) Electric field (top panels) and phase (bottom panels) distributions on the right-handed nanospirals by vortex beams with topological charges $l = \pm 9$. The circular arrows indicate the opposite azimuthal phase gradient generated by vortex beams.

matter interaction can also be obtained from the inversion-symmetry electromagnetic field distributions by flipping the chirality of OAM beams and structures simultaneously.

Experimental and Simulated HD Spectra of Planar Nanostructures. To excite a conspicuous chiroptical response in chiral metamaterials, we designed the single planar nanostructures with a comparable in-plane chiral feature to the vortex-beam size. The planar nanostructures were fabricated by direct laser writing in a commercial photoresist SZ2080 (see the Experimental Section for details).[42,43] The planar-chiral Archimedean nanospirals have a line width of $w = 420$ nm, $r_{max} = 2$ μm, and a thickness of $h = 2$ μm. Despite the same optical intensity profiles for incident optical vortices with topological charge $|\pm l|$ from 3 to 13, the right-handed nanostructure has a stronger reflection for $+l$ than $-l$, as shown in Figure 2a. In contrast, the situation of reflectance spectra is exactly interchanged for the left-handed nanostructure (Figure 2b). For the achiral cross-shaped nanostructure, no obvious difference is observed on the reflectance spectrum, as shown in Figure 2c. To theoretically analyze the origin of reflectance difference, all the numerically modeled results are simulated in the three types of nanostructures with the same dimensions as those of the fabricated samples by full electromagnetic finite-difference time-domain (FDTD) method (see more details in the Experimental section), as shown in Figure 2d−f. The line shapes of experimental measurements are in good agreement with numerical computed results, with differences coming from inhomogeneous geometrical line width, surface roughness, and the uncertainty in the optical measurements.

To further demonstrate the chiroptical phenomena on single nanostructures, we calculate the helical dichroism of the planar nanostructures as

$$HD = 2 \times (I_{+l} - I_{-l})/(I_{+l} + I_{-l})$$

where the subscripts indicate the topological charge of vortex beams.[44,45] The achiral nanostructure has a near-zero value on the HD spectrum (Figure 3a). For the chiral nanostructures, the simulated HD spectrum exhibits local peaks (valleys) at the topological charges $|\pm l| = 4$ and 9, as shown in Figure 3b. The maximum HD signal of $\sim$20% is achieved on the single right-handed nanostructure at the wavelength of 800 nm, where the spin-dependent CD signal of <0.5% is weak (see Figure S2). Furthermore, the HD value is positive (negative) for the right-handed (left-handed) nanospirals throughout the investigated regime, indicating a robust chiroptical response. The physical explanation of HD can be directly observed from the electromagnetic field simulations, where different optical intensity distributions are induced by vortex beams with opposite topological charges. For the right-handed nanospirals, there is a stronger electric field intensity by vortex beams with topological charge $l = +4$ than -4 (Figure 3c). Theoretically, the rotational symmetry of optical fields is dependent on the C_4 nanostructures. However, due to the linearly polarized states of incident vortex beams, the electric field distributions demonstrate a 2-fold rotational symmetry, which has no influence on the generation of HD. The strict C_4 symmetry of electric field distributions can be realized by cylindrical vector vortex beams with azimuthal or radial polarizations (see Figure S3).
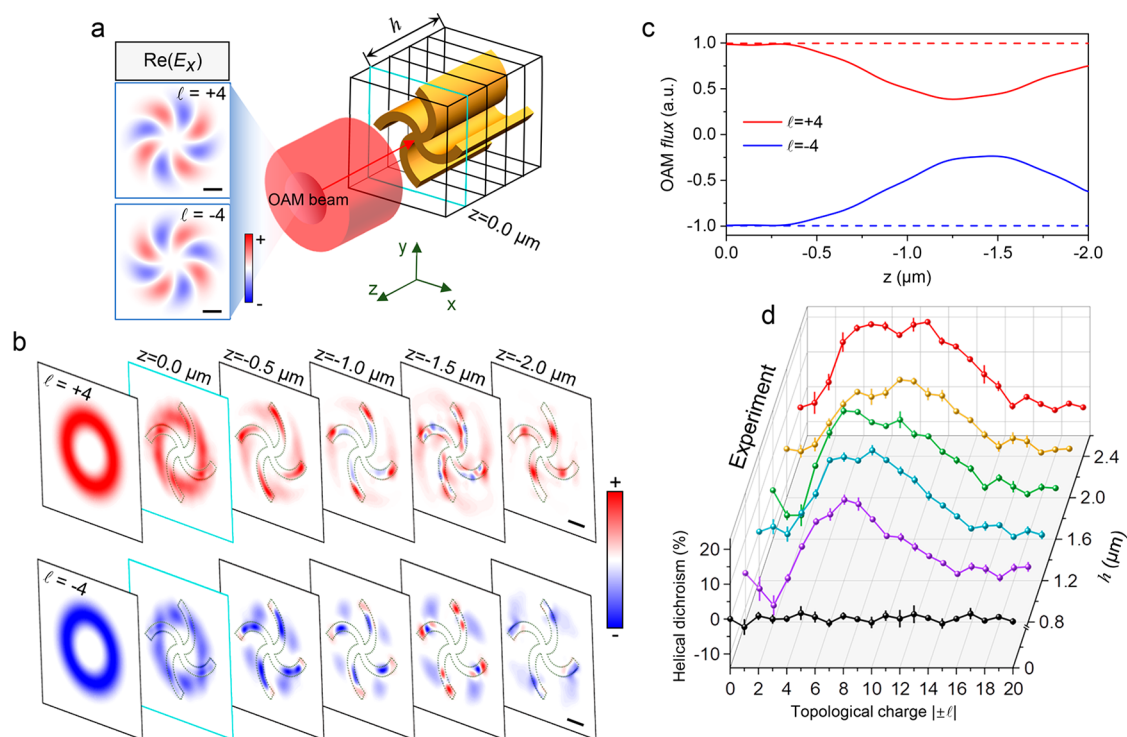
Figure 4. Chiroptical characterization of planar-chiral nanostructures with varying thickness. (a) Schematic of the single right-handed nanospirals with thickness h illuminated by OAM beams with topological charge $l = \pm 4$. Insets show the electric field distributions of OAM beams. (b) Simulated time-averaged OAM flux distributions at varied transversal planes along propagation direction $-z$ in (a). The transversal plane ($z = 0\ \mu$m) locates at the top surface of the right-handed nanostructure ($h = 2\ \mu$m). The color scale indicates the magnitude of the OAM flux, with red (blue) indicating a positive (negative) value. Scale bars in (a, b) are 1 μm. (c) OAM flux spectra as a function of z position in the right-handed nanospirals (solid lines) and free space (dashed lines). (d) Measured HD spectra of the right-handed nanospirals with different thickness. All the nanostructures have the same planar-chiral features.

More chiral nanostructures—for example, changing their rotational symmetry from C_3 to C_5—reveals the inherent robustness of HD response associated with their planar chirality (see Figure S4). Thanks to the odd-parity helicity, we also conclude that the HD sign of left-handed nanospirals is reversed, demonstrating the inversion-symmetric intensity distributions (Figure 3d). It is worth to note that the original counterclockwise or clockwise Poynting vectors in vortex beams are converted to identical chirality after interacting with chiral nanostructures (see Figure S5). To investigate the OAM-mode transformation on planar nanostructures, we also decomposed the OAM modes of electric fields to generate the discrete OAM spectra (see Figure S6). The OAM modes of light can be converted by the planar-chiral nanostructures, reminiscent of recently reported generation of OAM beams by chiral structures.[46−48] Figure 3e shows that the vortex beams, carrying larger topological charges $l = \pm 9$, can interact with the end of spiral lobes to induce the maximum HD signal. Intriguingly, distinguishing from the quasi-plane wave in CD measurements, the azimuthal phase distributions of vortex beams are obviously modulated by the chiral nanostructures, leading to varied OAM modes. It is also worth noting that CD spectroscopy of chiral metamaterials typically demands a lattice-constant factor comparable to the operating wavelength of interest for instigating plasmonic resonances,[37] whereas the vortex beams can directly interact with a single nanostructure to yield a pronounced HD signal (see Figure S7).

Optical Chirality Flux Demonstration of Nanostructures with Varying Thickness. To obtain pronounced chiroptical responses, chiral light is typically imbued in 3D materials, where the enantiomers twist with helical pitch of the light wave, in terms of rotation and propagating distance.[49] Although there generally is a smaller chiroptical signal in planar-chiral structures than 3D helical structures,[37] the HD response can still be enhanced by tuning the geometric parameters of planar-chiral structures. In particular, multiple planar structures can even be assembled to chiral building blocks for yielding a strong chiroptical response.[7,24,50] To provide insight into the thickness dependency of chiroptical response, we have investigated the time-averaged OAM flux in nanospirals along the propagation direction, as shown in Figure 4a. In free space, the OAM flux is bounded by the conservation law of optical chirality (see section S5).[51−53] After interacting with chiral nanostructures, the transversal OAM flux demonstrates disordered distributions for incident vortex beams (Figure 4b). The mirror symmetry of OAM flux for vortex beams with opposite topological charges $l = \pm 4$ is broken in the chiral systems (see Figure S8). The transmitted OAM fluxes have been normalized to that of vortex beam with topological charge $l = +4$. Analogous to the SAM fluxes in nanostructures,[52] the transmitted OAM fluxes are decreased after interacting with nanostructures, indicating a dissipation of chirality (Figure 4c). The quantity of chiroptical dissipation is dependent on the propagating length, leading to a tunable HD response by varying the thickness of nanostructures.

Figure 4d shows the experimentally measured HD spectra of right-handed nanospirals with varying thicknesses from 0.8 to 2.4 μm at a step of 0.4 μm. By tailoring the thickness of nanostructures, a robust chiroptical response is achieved on the HD spectra, further confirmed by the simulated results (see

Figure S9). As a result, we can also readily control the HD spectra of planar nanostructures by tuning their OAM fluxes. Note that the dielectric nanostructures used in our experiments are lossless with a refractive index of 1.51. The optical activity in the form of helical dichroism absorption can also be realized by using lossy materials (see Figure S10). Such a versatile chiroptical detection makes HD spectroscopy essential for detecting chiral materials in small quantities, yielding a high-sensitivity vortex-assisted chiroptical response even on the single nanostructures.

CONCLUSIONS

In summary, we have demonstrated the experimental observation and theoretical analysis of chiroptical manifestation on single planar nanostructures by OAM of light. The chiroptical signals in the form of HD can unambiguously distinguish the chirality of single planar-chiral nanostructures. The fully electromagnetic wave computational model confirms the mirror-symmetry chiroptical spectra between planar nanostructures with opposite handedness, revealing the relationship between geometric structures and optical activity. On the basis of these results, we expect that the high-sensitivity HD measurements can detect the optical activity of chiral matters in small quantities, which can significantly decrease the requirements of production efficiency. Additionally, the researches of chiroptical response in metamaterials, expanding to single nanostructures, can explore the chiral light-matter interactions by vortex beams, potentially applied in chiral quantum optics and next-generation chiroptical spectroscopy.

EXPERIMENTAL SECTION

Sample Preparation. The dielectric nanostructures used in our experiment were fabricated by direct laser writing in a commercially available zirconium−silicon hybrid sol−gel material (SZ2080, IESL-FORTH). Compared with other photoresists, the shrinkage of SZ2080 was negligible during structural processing. Before laser engineering, the prebaking process was set to a thermal platform at 100 °C for 45 min to evaporate the solvent in the material. After photopolymerization, the polymer material was developed in 1-propanol for 30 min until all the unpolymerized part was washed away.

Experimental Setup. A mode-locked Ti:sapphire ultrafast oscillator (Chameleon Vision-S, Coherent, Inc.) was used as the femtosecond laser source. The central wavelength of laser was 800 nm, with a pulse width of 75 fs and a repetition rate of 80 MHz. The phase-only reflective liquid-crystal SLM (Pluto NIR-2, Holoeye Photonics AG) has 1920×1080 pixels, with pixel pitch of 8 μm, on which computer-generated holograms with 256 gray levels can be displayed. A $60\times$ oil-immersed objective lens (NA = 1.35, Olympus) and a general $100\times$ dry objective lens (NA = 0.9, Olympus) were used in direct-laser-writing process and chiroptical detection, respectively. The sample was mounted on a 3D-piezo-nanostage (E545, Physik Instrumente) with nanoscale resolution and a 200 μm $\times$ 200 μm $\times$ 200 μm traveling range to precisely tune the locations of nanostructures under optical microscopy. The white light in microscopy was used for observing the precise position of nanostructures, which was switched off in reflectance measurements. The tailored vortex beams with various topological charge were focused on the nanowires at the normal incidence by the microscope objective.

Detection of Planar Nanostructures. The right-handed, left-handed, and achiral planar nanowires are precisely positioned for aligning to the generated vortex beam by the 3D-piezo-nanostage, respectively. After positioning the single nanostructure to the beam axes of optical vortices, the reflected intensity was caught by a CCD (MindVision HD-SUA133GM-T camera, image area: 1280×1024

pixels) with the acquisition time of 30 ms. For a single planar-chiral nanostructure, all optical images were gathered in 10 min for calculating its reflectance. The laser power of incident vortex beams was 0.5 mW for achieving clarified optical images on the CCD. The SEM images of nanostructures were taken by a secondary electron scanning electron microscope (ZEISS EVO18) with an accelerating voltage of 10 keV after depositing ∼10 nm gold on the sample.

Numerical Simulation. The numerical simulations were performed using a commercial finite difference time-domain-based software (Lumerical FDTD Solutions, Inc.). In the simulation, the refractive index of metamaterial was set to be 1.51. Perfectly matched layer boundaries were employed for the X, Y, and Z directions. The incident electrical field distribution of linearly polarized vortex beams is defined as

$$u_l(r, \varphi) = \frac{C}{\sqrt{|l|!}} r^{|l|} \exp\left(-\frac{r^2}{\omega_0^2}\right) \exp(il\varphi)\hat{x} \tag{2}$$

where C is a normalized constant, $\omega_0 = 2.05$ is the beam waist based on the experimental system, and (r, φ) is the polar coordinate system.

ASSOCIATED CONTENT

ⓢ Supporting Information

The Supporting Information is available free of charge at https://pubs.acs.org/doi/10.1021/acsnano.0c08941.

> Sections S1−S5: theoretical analysis of the CD response in single nanostructures, mirror-symmetric HD spectra, digital spiral spectra, FDTD simulations, angular-momentum flux; Figures S1−S10: SEM images of nanostructures, simulated CD spectrum, optical field by cylindrical vector vortex beams, HD spectra on nanostructures with different rotational symmetry, Poynting vectors map of vortex beams, discrete OAM spectra; schematic of CD on wavelength-scale nanostructures, OAM flux on the achiral nanostructure, simulated HD spectra on chiral nanostructures with varying thickness, HD and HD absorption spectra on lossy materials (PDF)

AUTHOR INFORMATION

Corresponding Authors

Jiawen Li − *CAS Key Laboratory of Mechanical Behavior and Design of Materials, Department of Precision Machinery and Precision Instrumentation, University of Science and Technology of China, Hefei, Anhui 230027, China;* ⓞ orcid.org/0000-0003-3950-6212; Email: jwl@ustc.edu.cn

Dong Wu − *CAS Key Laboratory of Mechanical Behavior and Design of Materials, Department of Precision Machinery and Precision Instrumentation, University of Science and Technology of China, Hefei, Anhui 230027, China;* ⓞ orcid.org/0000-0003-0623-1515; Email: dongwu@ustc.edu.cn

Cheng-Wei Qiu − *Department of Electrical and Computer Engineering, National University of Singapore, Singapore 117583, Singapore;* ⓞ orcid.org/0000-0002-6605-500X; Email: chengwei.qiu@nus.edu.sg

Authors

Jincheng Ni − *CAS Key Laboratory of Mechanical Behavior and Design of Materials, Department of Precision Machinery and Precision Instrumentation, University of Science and Technology of China, Hefei, Anhui 230027, China; Department of Electrical and Computer Engineering,*

National University of Singapore, Singapore 117583, Singapore; ⊙ orcid.org/0000-0001-9308-4511

Shunli Liu − *CAS Key Laboratory of Mechanical Behavior and Design of Materials, Department of Precision Machinery and Precision Instrumentation, University of Science and Technology of China, Hefei, Anhui 230027, China*

Guangwei Hu − *Department of Electrical and Computer Engineering, National University of Singapore, Singapore 117583, Singapore;* ⊙ orcid.org/0000-0002-3023-9632

Yanlei Hu − *CAS Key Laboratory of Mechanical Behavior and Design of Materials, Department of Precision Machinery and Precision Instrumentation, University of Science and Technology of China, Hefei, Anhui 230027, China;* ⊙ orcid.org/0000-0003-1964-0043

Zhaoxin Lao − *CAS Key Laboratory of Mechanical Behavior and Design of Materials, Department of Precision Machinery and Precision Instrumentation, University of Science and Technology of China, Hefei, Anhui 230027, China*

Qing Zhang − *Department of Electrical and Computer Engineering, National University of Singapore, Singapore 117583, Singapore*

Shaohua Dong − *Department of Electrical and Computer Engineering, National University of Singapore, Singapore 117583, Singapore*

Jiaru Chu − *CAS Key Laboratory of Mechanical Behavior and Design of Materials, Department of Precision Machinery and Precision Instrumentation, University of Science and Technology of China, Hefei, Anhui 230027, China;* ⊙ orcid.org/0000-0001-6472-8103

Complete contact information is available at:
https://pubs.acs.org/10.1021/acsnano.0c08941

Author Contributions

[§]J.N. and S.L. contributed equally to this work. J.N. and C.W.Q. conceived the idea and developed the theory. J.N., Q.Z., S.D., and G.H. performed the simulations. J.N. and S.L. performed the experiments. J.N., J.L., D.W., J.C., and Z.L. analyzed the data. J.N., C.W.Q., and D.W. wrote the manuscript. C.W.Q. and D.W. supervised the project. All authors discussed the results and commented on the manuscript.

Notes

The authors declare no competing financial interest.

REFERENCES

(1) Rao, Z.; Li, H.; Zhang, T.; Tian, S.; Li, C.; Fu, B.; Tang, C.; Wang, L.; Li, Z.; Fan, W. Observation of Unconventional Chiral Fermions with Long Fermi Arcs in CoSi. *Nature* **2019**, *567*, 496−499.

(2) Davis, M. S.; Zhu, W.; Lee, J. K.; Lezec, H. J.; Agrawal, A. Microscopic Origin of the Chiroptical Response of Optical Media. *Sci. Adv.* **2019**, *5*, No. eaav8262.

(3) Gansel, J. K.; Thiel, M.; Rill, M. S.; Decker, M.; Bade, K.; Saile, V.; von Freymann, G.; Linden, S.; Wegener, M. Gold Helix Photonic Metamaterial as Broadband Circular Polarizer. *Science* **2009**, *325*, 1513−1515.

(4) Kuzyk, A.; Schreiber, R.; Fan, Z. Y.; Pardatscher, G.; Roller, E. M.; Hogele, A.; Simmel, F. C.; Govorov, A. O.; Liedl, T. DNA-Based Self-Assembly of Chiral Plasmonic Nanostructures with Tailored Optical Response. *Nature* **2012**, *483*, 311−314.

(5) Frenzel, T.; Kadic, M.; Wegener, M. Three-Dimensional Mechanical Metamaterials with a Twist. *Science* **2017**, *358*, 1072−1074.

(6) Mark, A. G.; Gibbs, J. G.; Lee, T. C.; Fischer, P. Hybrid Nanocolloids with Programmed Three-Dimensional Shape and Material Composition. *Nat. Mater.* **2013**, *12*, 802−807.

(7) Hentschel, M.; Schaferling, M.; Duan, X. Y.; Giessen, H.; Liu, N. Chiral Plasmonics. *Sci. Adv.* **2017**, *3*, No. e1602735.

(8) Bliokh, K. Y.; Rodriguez-Fortuno, F. J.; Nori, F.; Zayats, A. V. Spin-Orbit Interactions of Light. *Nat. Photonics* **2015**, *9*, 796−808.

(9) Allen, L.; Beijersbergen, M. W.; Spreeuw, R. J. C.; Woerdman, J. P. Orbital Angular-Momentum of Light and the Transformation of Laguerre-Gaussian Laser Modes. *Phys. Rev. A: At., Mol., Opt. Phys.* **1992**, *45*, 8185−8189.

(10) Zhang, Z.; Qiao, X.; Midya, B.; Liu, K.; Sun, J.; Wu, T.; Liu, W.; Agarwal, R.; Jornet, J. M.; Longhi, S. Tunable Topological Charge Vortex Microlaser. *Science* **2020**, *368*, 760−763.

(11) Chong, A.; Wan, C.; Chen, J.; Zhan, Q. Generation of Spatiotemporal Optical Vortices with Controllable Transverse Orbital Angular Momentum. *Nat. Photonics* **2020**, *14*, 350−354.

(12) Ni, J. C.; Wang, Z. Y.; Li, Z. Q.; Lao, Z. X.; Hu, Y. L.; Ji, S. Y.; Xu, B.; Zhang, C. C.; Li, J. W.; Wu, D.; Chu, J. R. Multifurcate Assembly of Slanted Micropillars Fabricated by Superposition of Optical Vortices and Application in High-Efficiency Trapping Microparticles. *Adv. Funct. Mater.* **2017**, *27*, 1701939.

(13) Qiu, C.-W.; Yang, Y. Vortex Generation Reaches a New Plateau. *Science* **2017**, *357*, 645−645.

(14) Hu, Y.; Wang, Z.; Wang, X.; Ji, S.; Zhang, C.; Li, J.; Zhu, W.; Wu, D.; Chu, J. Efficient Full-Path Optical Calculation of Scalar and Vector Diffraction Using the Bluestein Method. *Light: Sci. Appl.* **2020**, *9*, 1−11.

(15) Banerjee-Ghosh, K.; Dor, O. B.; Tassinari, F.; Capua, E.; Yochelis, S.; Capua, A.; Yang, S.-H.; Parkin, S. S.; Sarkar, S.; Kronik, L. Separation of Enantiomers by Their Enantiospecific Interaction with Achiral Magnetic Substrates. *Science* **2018**, *360*, 1331−1334.

(16) Mun, J.; Kim, M.; Yang, Y.; Badloe, T.; Ni, J.; Chen, Y.; Qiu, C.-W.; Rho, J. Electromagnetic Chirality: from Fundamentals to Nontraditional Chiroptical Phenomena. *Light: Sci. Appl.* **2020**, *9*, 1−18.

(17) Sharma, V.; Crne, M.; Park, J. O.; Srinivasarao, M. Structural Origin of Circularly Polarized Iridescence in Jeweled Beetles. *Science* **2009**, *325*, 449−451.

(18) Hu, Y.; Yuan, H.; Liu, S.; Ni, J.; Lao, Z.; Xin, C.; Pan, D.; Zhang, Y.; Zhu, W.; Li, J. Chiral Assemblies of Laser-Printed Micropillars Directed by Asymmetrical Capillary Force. *Adv. Mater.* **2020**, *32*, 2002356.

(19) Esposito, M.; Tasco, V.; Todisco, F.; Cuscuna, M.; Benedetti, A.; Sanvitto, D.; Passaseo, A. Triple-Helical Nanowires by Tomographic Rotatory Growth for Chiral Photonics. *Nat. Commun.* **2015**, *6*, 6484.

(20) Zhang, Q. F.; Hernandez, T.; Smith, K. W.; Jebeli, S. A. H.; Dai, A. X.; Warning, L.; Baiyasi, R.; McCarthy, L. A.; Guo, H.; Chen, D. H.; Dionne, J. A.; Landes, C. F.; Link, S. Unraveling the Origin of

Chirality from Plasmonic Nanoparticle-Protein Complexes. *Science* **2019**, *365*, 1475−1478.

(21) Chen, Y.; Yang, X.; Gao, J. 3D Janus Plasmonic Helical Nanoapertures for Polarization-Encrypted Data Storage. *Light: Sci. Appl.* **2019**, *8*, 1−9.

(22) Kerber, R.; Fitzgerald, J.; Oh, S.; Reiter, D.; Hess, O. Orbital Angular Momentum Dichroism in Nanoantennas. *Commun. Phys.* **2018**, *1*, 1−7.

(23) Zambrana-Puyalto, X.; Vidal, X.; Molina-Terriza, G. Angular Momentum-Induced Circular Dichroism in Non-Chiral Nanostructures. *Nat. Commun.* **2014**, *5*, 4922.

(24) Zhao, Y.; Belkin, M. A.; Alù, A. Twisted Optical Metamaterials for Planarized Ultrathin Broadband Circular Polarizers. *Nat. Commun.* **2012**, *3*, 870.

(25) Ni, J. C.; Wang, C. W.; Zhang, C. C.; Hu, Y. L.; Yang, L.; Lao, Z. X.; Xu, B.; Li, J. W.; Wu, D.; Chu, J. R. Three-Dimensional Chiral Microstructures Fabricated by Structured Optical Vortices in Isotropic Material. *Light: Sci. Appl.* **2017**, *6*, No. e17011.

(26) Hu, G.; Hong, X.; Wang, K.; Wu, J.; Xu, H.-X.; Zhao, W.; Liu, W.; Zhang, S.; Garcia-Vidal, F.; Wang, B. Coherent Steering of Nonlinear Chiral Valley Photons with a Synthetic Au-WS$_2$ Metasurface. *Nat. Photonics* **2019**, *13*, 467−472.

(27) Li, G.; Zhang, S.; Zentgraf, T. Nonlinear Photonic Metasurfaces. *Nat. Rev. Mater.* **2017**, *2*, 1−14.

(28) Chen, S.; Zeuner, F.; Weismann, M.; Reineke, B.; Li, G.; Valev, V. K.; Cheah, K. W.; Panoiu, N. C.; Zentgraf, T.; Zhang, S. Giant Nonlinear Optical Activity of Achiral Origin in Planar Metasurfaces with Quadratic and Cubic Nonlinearities. *Adv. Mater.* **2016**, *28*, 2992−2999.

(29) Collins, J. T.; Hooper, D. C.; Mark, A. G.; Kuppe, C.; Valev, V. K. Second-Harmonic Generation Optical Rotation Solely Attributable to Chirality in Plasmonic Metasurfaces. *ACS Nano* **2018**, *12*, 5445−5451.

(30) Hendry, E.; Carpy, T.; Johnston, J.; Popland, M.; Mikhaylovskiy, R. V.; Lapthorn, A. J.; Kelly, S. M.; Barron, L. D.; Gadegaard, N.; Kadodwala, M. Ultrasensitive Detection and Characterization of Biomolecules Using Superchiral Fields. *Nat. Nanotechnol.* **2010**, *5*, 783−787.

(31) Menzel, C.; Helgert, C.; Rockstuhl, C.; Kley, E.-B.; Tünnermann, A.; Pertsch, T.; Lederer, F. Asymmetric Transmission of Linearly Polarized Light at Optical Metamaterials. *Phys. Rev. Lett.* **2010**, *104*, 253902.

(32) Fedotov, V.; Schwanecke, A.; Zheludev, N.; Khardikov, V.; Prosvirnin, S. Asymmetric Transmission of Light and Enantiomerically Sensitive Plasmon Resonance in Planar Chiral Nanostructures. *Nano Lett.* **2007**, *7*, 1996−1999.

(33) Wu, S.; Zhang, Z.; Zhang, Y.; Zhang, K.; Zhou, L.; Zhang, X.; Zhu, Y. Enhanced Rotation of the Polarization of a Light Beam Transmitted through a Silver Film with an Array of Perforated S-Shaped Holes. *Phys. Rev. Lett.* **2013**, *110*, 207401.

(34) Khanikaev, A. B.; Arju, N.; Fan, Z.; Purtseladze, D.; Lu, F.; Lee, J.; Sarriugarte, P.; Schnell, M.; Hillenbrand, R.; Belkin, M. Experimental Demonstration of the Microscopic Origin of Circular Dichroism in Two-Dimensional Metamaterials. *Nat. Commun.* **2016**, *7*, 1−8.

(35) Plum, E.; Liu, X. X.; Fedotov, V. A.; Chen, Y.; Tsai, D. P.; Zheludev, N. I. Metamaterials: Optical Activity without Chirality. *Phys. Rev. Lett.* **2009**, *102*, 113902.

(36) Ren, M.; Plum, E.; Xu, J.; Zheludev, N. I. Giant Nonlinear Optical Activity in a Plasmonic Metamaterial. *Nat. Commun.* **2012**, *3*, 833.

(37) Zhu, A. Y.; Chen, W. T.; Zaidi, A.; Huang, Y.-W.; Khorasaninejad, M.; Sanjeev, V.; Qiu, C.-W.; Capasso, F. Giant Intrinsic Chiro-Optical Activity in Planar Dielectric Nanostructures. *Light: Sci. Appl.* **2018**, *7*, 17158.

(38) Feng, W. C.; Kim, J. Y.; Wang, X. Z.; Calcaterra, H. A.; Qu, Z. B.; Meshi, L.; Kotov, N. A. Assembly of Mesoscale Helices with Near-Unity Enantiomeric Excess and Light-Matter Interactions for Chiral Semiconductors. *Sci. Adv.* **2017**, *3*, No. e1601159.

(39) Lee, H. E.; Ahn, H. Y.; Mun, J.; Lee, Y. Y.; Kim, M.; Cho, N. H.; Chang, K.; Kim, W. S.; Rho, J.; Nam, K. T. Amino-Acid- and Peptide-Directed Synthesis of Chiral Plasmonic Gold Nanoparticles. *Nature* **2018**, *556*, 360−365.

(40) Kuznetsov, A. I.; Miroshnichenko, A. E.; Brongersma, M. L.; Kivshar, Y. S.; Luk'yanchuk, B. Optically Resonant Dielectric Nanostructures. *Science* **2016**, *354*, No. aag2472.

(41) Chen, L.; Lei, J.; Romero, J. Quantum Digital Spiral Imaging. *Light: Sci. Appl.* **2014**, *3*, No. e153.

(42) Ji, S. Y.; Yang, L.; Zhang, C. C.; Cai, Z.; Hu, Y. L.; Li, J. W.; Wu, D.; Chu, J. R. High-Aspect-Ratio Microtubes with Variable Diameter and Uniform Wall Thickness by Compressing Bessel Hologram Phase Depth. *Opt. Lett.* **2018**, *43*, 3514−3517.

(43) Lao, Z. X.; Hu, Y. L.; Pan, D.; Wang, R. Y.; Zhang, C. C.; Ni, J. C.; Xu, B.; Li, J. W.; Wu, D.; Chu, J. R. Self-Sealed Bionic Long Microchannels with Thin Walls and Designable Nanoholes Prepared by Line-Contact Capillary-Force Assembly. *Small* **2017**, *13*, 1603957.

(44) Brullot, W.; Vanbel, M. K.; Swusten, T.; Verbiest, T. Resolving Enantiomers Using the Optical Angular Momentum of Twisted Light. *Sci. Adv.* **2016**, *2*, No. e1501349.

(45) Ni, J.; Liu, S.; Wu, D.; Lao, Z.; Wang, Z.; Huang, K.; Ji, S.; Li, J.; Huang, Z.; Xiong, Q. Gigantic Vortical Differential Scattering as a Monochromatic Probe for Multiscale Chiral Structures. *Proc. Natl. Acad. Sci. U. S. A.* **2021**, *118*, No. e2020055118.

(46) Spektor, G.; Kilbane, D.; Mahro, A.; Frank, B.; Ristok, S.; Gal, L.; Kahl, P.; Podbiel, D.; Mathias, S.; Giessen, H. Revealing the Subfemtosecond Dynamics of Orbital Angular Momentum in Nanoplasmonic Vortices. *Science* **2017**, *355*, 1187−1191.

(47) Yang, Y.; Thirunavukkarasu, G.; Babiker, M.; Yuan, J. Orbital-Angular-Momentum Mode Selection by Rotationally Symmetric Superposition of Chiral States with Application to Electron Vortex Beams. *Phys. Rev. Lett.* **2017**, *119*, 094802.

(48) Sun, W.; Liu, Y.; Qu, G.; Fan, Y.; Dai, W.; Wang, Y.; Song, Q.; Han, J.; Xiao, S. Lead Halide Perovskite Vortex Microlasers. *Nat. Commun.* **2020**, *11*, 1−7.

(49) Rodrigues, S. P.; Lan, S.; Kang, L.; Cui, Y.; Panuski, P. W.; Wang, S.; Urbas, A. M.; Cai, W. Intensity-Dependent Modulation of Optically Active Signals in a Chiral Metamaterial. *Nat. Commun.* **2017**, *8*, 1−8.

(50) Decker, M.; Ruther, M.; Kriegler, C.; Zhou, J.; Soukoulis, C.; Linden, S.; Wegener, M. Strong Optical Activity from Twisted-Cross Photonic Metamaterials. *Opt. Lett.* **2009**, *34*, 2501−2503.

(51) Bliokh, K. Y.; Dressel, J.; Nori, F. Conservation of the Spin and Orbital Angular Momenta in Electromagnetism. *New J. Phys.* **2014**, *16*, 093037.

(52) Gilroy, C.; Hashiyada, S.; Endo, K.; Karimullah, A. S.; Barron, L. D.; Okamoto, H.; Togawa, Y.; Kadodwala, M. Roles of Superchirality and Interference in Chiral Plasmonic Biodetection. *J. Phys. Chem. C* **2019**, *123*, 15195−15203.

(53) Poulikakos, L. V.; Gutsche, P.; McPeak, K. M.; Burger, S.; Niegemann, J.; Hafner, C.; Norris, D. J. Optical Chirality Flux as a Useful Far-Field Probe of Chiral Near Fields. *ACS Photonics* **2016**, *3*, 1619−1625.